SPATIALLY RESOLVED ANALYSIS OF SELECTIVELY DOPED REGIONS VIA CONFOCAL RAMAN MICROSCOPY

A. Herguth, J. Ebser, D. Sommer, S. Ohl, B. Terheiden, G. Hahn
University of Konstanz, Department of Physics, 78457 Konstanz, Germany

ABSTRACT: More or less all proposed highly efficient solar cell concepts use quite successfully laterally selective boron doping. However, quality control regarding achieved doping level, lateral extension, etc. on real devices or precursors gets more and more complicated with these small structures as the typical characterisation techniques simply do not work well on small scale. High resolution mapping confocal Raman spectroscopy is considered a possible technique to tackle this challenge. In this contribution it is demonstrated on IBC precursor structures that the contrast in local doping level can be finely resolved via mapping Raman spectroscopy, even though the determined absolute value is found to be too small. It is discussed on the basis of a few fundamental calculations that the depth sensitivity is accountable for this drawback.
Keywords: boron, doping, characterization

1 INTRODUCTION

In the past decade the achievable efficiency of crystalline silicon solar cells in industrial mass production has risen (at least for Cz-grown substrates) from below 15% to around 20% (non-PERx technology, Passivated Emitter and Rear) with perspective towards maybe 22% (PERx technology) in the next years. One of the key features of this development was the insight that the surface doping requirements for an adequate metal-silicon contact differ strongly from those for an excellent surface passivation. This triggered the development of spatial selective doping, be it a selective emitter, selective front and back surface fields or local contacts disrupting a dielectrically passivated surface.

Finally, this development culminates in the strongly patterned architecture used for interdigitated back contact (IBC) concepts or alike with demonstrated efficiencies exceeding 23%.

Even though spatially inhomogeneous doping may promise a higher efficiency potential, it is by far more challenging to control the quality of the process as the doped regions may extend only a hundred microns or less in some cases, and standard techniques for doping (profile) control like four point probe, eddy current or ECV (Electochemical Capacitance Voltage) profiling simply do not work reliably on these small areas.

A common way to circumvent that problem is to co-process samples especially prepared with larger doped areas for these techniques. However, this does not work if upscaling these areas changes their properties as it is encountered, e.g., when preparing (wet) chemically small structures or using liquid-deposited doping sources. Due to the liquid's surface tension, the surface wettability and morphology, the exact thickness and other properties can depend on the size of the prepared structures.

Therefore, alternative techniques are sought-after which can be applied to the original structure at best without even compromising the sample and which are capable of mapping the local doping level qualitatively and quantitatively.

Confocal Raman microscopy is considered a promising candidate at least for p^+ layers as it offers a good resolution, surface sensitivity and is non-destructive. The sample can even be covered with a dielectric layer (for passivation purposes), as long as it is transparent enough for the excitation laser and the Stokes scattered light.

2 DOPING LEVEL AND RAMAN SPECTROSCOPY

It is well known that vibration modes/phonons in solids can interact with incoming photons, and energy transfer may occur: the Raman effect shifting the incoming light in wavelength. If, in addition, a multitude of electronically excitable energy states exists, as it is given in a partially empty valence band or partially filled conduction band, the phonons may couple to the charge carriers: a Fano resonance occurs. In that case the photon not only can exchange energy with a phonon but also with the electronic system. However, even though the interaction with electrons in the conduction band is principally possible, the photon/phonon/hole interaction is more pronounced and easier to observe.

As for the Raman effect alone, the probability for energy transfer from the photon to the phonon/electronic system is higher (Stokes scattering) than the other way around, and its probability drops with rising energy. In other words: it is more likely that the photon looses (in addition to the phonon excitation energy) only a small amount of energy to a carrier than losing much, and it is less probable that the photon gains energy from a carrier as it would require an already (thermally) excited carrier.

Thus Fano resonances imply that the Stokes scattered Raman peak features an asymmetric shape with a specific deformation for higher wavenumbers as shown Fig. 1.

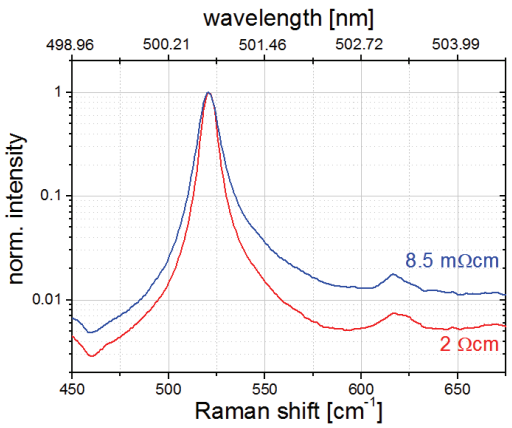

Fig. 1: Spectra showing the wavelength shift due to Raman scattering with the phononic and electronic system. The peak exhibits a stronger asymmetric shape for higher doping due to the additional interaction with the electronic system.

The exact shape of the peak depends on the multitude of electronically excitable states (e.g., the emptiness of the valence band and density of states) and thus –without strong carrier injection– on the doping level. Therefore, higher doped material exhibits a stronger asymmetry in Fig. 1. As it is derived by Becker et al. [1], the normalized spectral intensity I/I_0 of the peak may be described by

$$\frac{I(\Omega,q,\Gamma,\Omega_m)}{I_0}=\frac{\left[q+2(\Omega-\Omega_m)/\Gamma\right]^2}{1+\left[2(\Omega-\Omega_m)/\Gamma\right]^2} \qquad (1)$$

with Ω the wavenumber, Ω_m the peak position, Γ the (Lorentzian) linewidth and q a dimensionless parameter quantifying the Fano resonances and therefore the doping level. It is found that the doping level is–at least for highly doped silicon–proportional to 1/q and thus Eqn. 1 allows a determination of the doping level after the proportionality factor has been extracted from samples with known doping level.

For homogeneously doped bulk samples this procedure seems straight forward. However, p^+ layers are typically in-diffused by different techniques and exhibit a certain depth profile, e.g., following an error function sometimes with surface pile up/down, and a limited depth typically in the range of 0.5-1 µm. Therefore, the question arises what the influence of limited p^+ layer thickness is.

3 DEPTH SENSITIVITY

Generally speaking the measured signal is a convolution of different factors: the local laser intensity (the scattered intensity scales linearly with it), the escape probability of the scattered photons, and the probability of collecting these with the spectrometer (called in the following sensitivity).

The exact description of the various factors is tricky; however, a few simple approximations shall be made to show the general behavior.

In µ-Raman spectroscopy, the laser is focused on/in the sample and, if high lateral resolution is of interest, a high magnification with a high numerical aperture (NA) is used. This implies that the impinging light comes from a large angular range, in our case with NA 0.9 from angles even exceeding 60° (measured to the surface normal). But a simple estimation with Snellius' law shows that the light enters in a far smaller angle due to the high refractive index of silicon. The light is more or less channeled into the silicon. Therefore, the approximation of light incident perpendicularly on the surface can be made although it also means that there is virtually no focus plane.

With this approximation the incoming laser intensity I is dampened only with depth z by absorption (coefficient α_L) according to Beer-Lambert's law

$$I \propto \exp(-\alpha_L z) \qquad (2)$$

For the (Raman) scattered photons, the absorption is also the major loss source and thus one may state that the escape probability E scales also with Beer-Lambert's law

$$E \propto \exp(-\alpha_R z) \qquad (3)$$

This time, the absorption coefficient α_R of the Raman scattered light has to be used, however, the change in wavelength is rather small and thus α_R is not far from α_L.

The product of both factors then scales with the sum of the absorption coefficients and thus the probability to receive a scattered photon from depth z scales with the characteristic length roughly being half of the laser's absorption length.

$$I \cdot E \propto \exp\left[-(\alpha_L+\alpha_R)z\right] \approx \exp(-2\alpha_L z) \qquad (4)$$

The sensitivity is a very difficult thing to assess as it includes the whole beam path in the confocal microscope. In general, it has to be noted that it is not possible to project an infinitely small light source through the optical system without entering the refraction regime of wave optics and in consequence the projected image of the point source is spread in space (point spread function). Vice versa, the projection through the microscope onto the fiber core (the confocal pinhole) suffers from the same limitation and thus a finite ellipsoidal space region is projected onto the fiber core. The radial extension is given by the used laser and optics and of the order of 300-500 nm (FWHM) allowing for a high lateral resolution. This high sensitivity is not transferable to the axial direction. As mentioned before, the high refractive index of silicon leads to a "channeling" of the incoming light and this also holds for the outgoing scattered light. In consequence, the axial extension of the sensitivity ellipsoid is by far larger than the radial extension and is around 5 µm. It should be noted here that the values are not to be considered true values but rather optimistic estimations to show the approximate dimensions.

If the characteristic length of the used laser is short compared to the axial extension of the sensitivity ellipsoid, the sensitivity S can be regarded as constant with depth z. The absorption length $1/\alpha_L$ of the used 488 nm laser is around 1 µm so that the characteristic length is around 0.5 µm being much smaller than the axial extension of the sensitivity ellipsoid and therefore the aforementioned approximation seems acceptable.

The signal strength from a certain depth is the product of all factors and scales approximately like Eqn. 4. The measured spectrum $\Phi(\Delta\lambda)$ is the depth integral of $I \cdot E \cdot S$ and the spectral shape $R(\Delta\lambda,h^+)$ of the scattering process being dependent on the local hole density (profile) $h^+(z)$

$$\Phi(\Delta\lambda)=\int R\left(\Delta\lambda,h^+(z)\right)\cdot I \cdot E \cdot S\, dz \qquad (5)$$

With Eqn. 4 it can be stated that in the case of a non-constant doping profile the measured spectrum is a depth-weighted mean.

It also can be stated that the signal contribution from the first characteristic length as defined in Eqn. 4 is only 63%, i.d., originates in our case from the first 0.5 µm. If the p^+ layer under investigation is only 0.5 µm thick, a non negligible contribution comes from the by far weaker doped substrate beneath. This is also illustrated in Fig. 2 for a typical diffused BBr_3 based emitter layer. The graph shows also that calculated signal strength including focusing varies with focal plane depth which is not perfectly compatible with the approximation of perpendicularly impinging light, but the flat curve near the surface shows that focusing has only small influence.

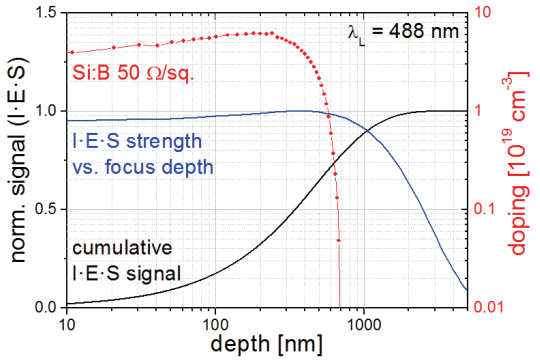

Fig. 2: Cumulative $I \cdot E \cdot S$ product with depth z compared to a typical BBr_3 based diffused p^+ depth profile. Also shown is the calculated signal strength including the focusing effect indicating that maximum signal is obtained with a focal plane being below the surface.

Both effects–the depth profile as well as the finite thickness–lead to a disturbed spectral shape compared to Eqn. 1 and a misinterpretation/underestimation of the determined doping level when Eqn. 1 is applied without corrections. Nevertheless, this so determined apparent doping is a valuable tool for device analysis as it still clearly shows where p^+ doping is present even though the determined value is too small.

4 LATERAL MAPPING OF DOPED REGIONS

In order to demonstrate the capabilities of µ-Raman spectroscopy regarding the imaging and quantification of laterally structured p^+ doped regions, an IBC precursor structure was used. A boron containing ink was inkjet-printed in a stripe pattern on a FZ-grown silicon wafer that was acidic etched prior to printing. The sample was exposed to high temperatures to allow for an in-diffusion of boron into the silicon substrate in order to form a p^+ layer. Prior to removing the ink residues, a dot pattern was engraved by laser for orientation purposes and microscope images were taken.

The Raman measurements were carried out with an Alpha 300 fiber coupled confocal Raman microscope from WITec featuring three excitation lasers (633 nm, 532 nm and 488 nm) with adjustable power. The actual depth and lateral resolution is adjustable by the magnification (up to ×100) and the fiber core (down to 25 µm). The CCD's spectral resolution is around 0.5 cm^{-1} within the region under investigation. The 488 nm laser was chosen for the measurements as it features the shortest absorption length and thus the best surface sensitivity.

A µ-Raman linescan was taken perpendicular to the stripe pattern with low magnification and thus relatively low lateral confocal resolution. In this case of low magnification, the focus plane has not to be corrected for each point as a few microns of sample height variation along the 2.5 µm line due to surface roughness and sample tilt are not found critical. The determined asymmetry factor was compared to homogeneously doped samples in the 10^{19} cm^{-3} range and the apparent doping was deduced. The result is shown in Fig. 3. As expected, the determined apparent doping is too small as compared to large area reference ECV measurements. Nevertheless, the values depict the correct range and show a clear transition between p^+ and non-p^+ doped regions. The transition region spans a few data points corresponding to a few microns. However, the chosen low magnification results in a lateral confocal sensitivity of a few microns and thus one can conclude that the transition is more abrupt than depicted in Fig. 3, but the true width cannot be determined for sure from this measurement.

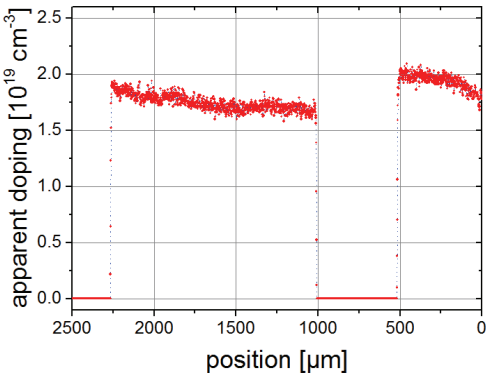

Fig. 3: Determined apparent doping along a line crossing p^+ and non-p^+ doped stripes. The data was taken with low magnification resulting in a lateral confocal resolution somewhat smaller 10 µm; step size was chosen to 1 µm.

In order to clarify which resolution can be reached with the used µ-Raman system, a small section comprising the transition region was selected and mapped with high magnification and a step width of 2 µm. In this case, the height had to be adjusted by auto-focusing meaning the height was adjusted to the maximum signal intensity. The result is shown in Fig. 4 as an overlay of the microscope image and apparent doping map. Note that the ink residues still visible in the microscope image were removed prior to µ-Raman imaging.

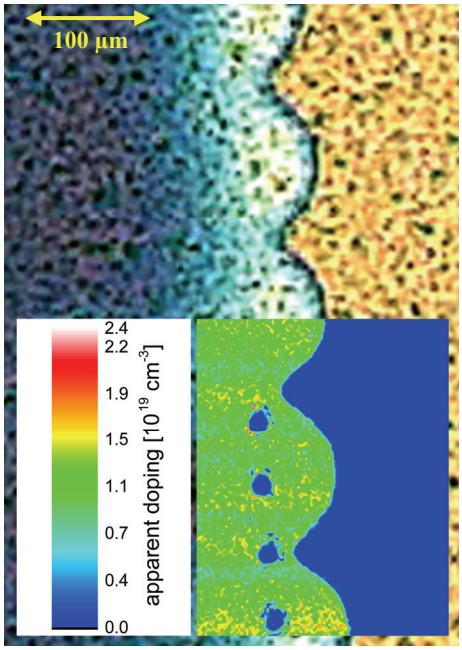

Fig. 4: Overlay of the microscope image and the determined apparent doping map. The four blue spots in a row are the engraved dots for orientation purposes. Slight stability problems of the used system are visible as horizontal stripes of deviating color/doping.

In this measurement the transition between p^+ and non-p^+ region comprises one pixel only, demonstrating well the high resolution capability of the used µ-Raman system. The former ink edge exhibits a curved shape due to the subsequent deposition of single drops merging perfectly with each other in the ink-jetted area, but in some places the drop pattern is still clearly recognizable at the edge.

5 SUMMARY

In this contribution the fundamental properties of confocal µ-Raman spectroscopy regarding depth sensitivity were exemplarily pointed out. The correct quantification of the doping level still seems challenging as the measured spectrum is a convolution of different factors not exactly known. Nevertheless, µ-Raman spectroscopy has proven to be capable of imaging lateral structured p^+ layers encountered, e.g., in IBC solar cells and may be used as a contact-free non-destructive characterization technique to identify doping production failures.

ACKNOWLEDGEMENTS

The authors would like to thank S. Joos for technical support during data post processing and IT assistance. Part of this work was financially supported by the German Federal Ministry for the Environment, Nature Conservation and Nuclear Safety (FKZ 0325581). The content of this publication is in the responsibility of the authors.

REFERENCES

[1] M. Becker et al., J. Appl. Phys. **106**, 074515 (2009) doi:10.1063/1.3236571.